SANS Investigations of Topological Constraints and Microscopic Deformations in Rubberelastic Networks

E. Straube

Martin-Luther-Universität Halle-Wittenberg, Fachbereich Physik, D-06099 Halle, Germany

V. Urban, W. Pyckhout-Hintzen,* and D. Richter

Forschungszentrum Jülich, Institut für Festkörperforschung, Postfach 1913, D-52425 Jülich, Germany

Received April 4, 1994; Revised Manuscript Received August 27, 1994[⊗]

ABSTRACT: The form factor of a labeled chain randomly cross-linked into a network in a tubelike approach is presented. Within a harmonic approximation for the constraining potential, the action of cross-links and entanglements is modeled by an effective tube, which is deformation dependent. The only parameters of the model are the reduced microscopic deformation, following a power law in the strain, and the diameter of the tube, which is inversely proportional to the strength of the constraints. First experimental results on polybutadiene networks with varying cross-link density are discussed. The conclusions drawn confirm a less than affine deformation at the molecular level while segmental fluctuations are found to be unperturbed despite the network topology and of the same size as obtained from rheology.

1. Introduction

The difficult problem of a detailed understanding of rubber elasticity can benefit from the consideration of mechanical (including thermodynamical) properties together with the form factor $S(\vec{k})$ of a single chain inside the polymer network. The wave vector range of the small-angle neutron scattering (SANS) allows the investigation of the chain deformation and of chain fluctuations on a length scale which is suitable for a test of crucial assumptions of current theories of rubber elasticity.

This is of special importance because recent developments are still approximate and the results of stress–strain experiments cannot decide conclusively between the numerous concepts.[1–3] Different realizations of one theoretical concept (e.g., the tube and the slip-link models for the entanglement concept[1]) but also different theoretical concepts (e.g., network models with orientation-dependent interactions[4]) are able to describe the stress–strain behavior of a large number of uniaxial extension experiments with comparable accuracy. The use of other modes of deformation (e.g., biaxial extension) would be very valuable, but experimental data are not available to the necessary extent. Tests of network theories using uniaxial stress–strain data only give useful information if the following three criteria are applied: (i) the given theory describes the stress–strain data of all rubberelastic networks with comparable accuracy, (ii) the model parameters deduced from fits of experimental data are compatible with the assumptions of the theory and with data obtained by independent methods, and (iii) the cross-link density derived from fit parameters of a given model agrees with values known from network buildup or other data.

In this way, it turned out that, e.g., the stress–strain behavior of networks made by cross-linking of long primary chains in bulk cannot be described within the whole range of investigated cross-link densities by the concept of restricted junction fluctuations.[1] On the other hand, it was proved that the slip-link model gives a very precise description of uniaxial stress–strain data but unrealistic cross-link densities.[6] Applying the above-mentioned criteria, however, it has been shown recently that only the tube model with deformation-dependent tube dimensions describes stress–strain data consistently. Additionally, over a large range of cross-link densities a very satisfactory agreement was achieved with data obtained from the network buildup and by spectroscopic methods.[1,5,6,7]

This model contains only two parameters which are not determined by the theory itself and which cannot be deduced completely independent from stress–strain data. These parameters are a numerical factor (α) which determines the strength of the constraints and a parameter (β) which describes the relaxation of the microscopic deformation of the network chains in comparison to the macroscopic deformation of the sample. This loss of affineness was introduced to understand the large variations of the constraint contributions to the network modulus which depends on the structure of the networks[1] and is discussed in a similar manner to explain SANS data of networks.[8]

Stress–strain data can be described within the tube model by values of these parameters which are in very satisfactory agreement with theoretical results or with the general assumptions of the theory, respectively. But a unique determination of these parameters from stress–strain data is limited by the fact that different sets of parameters may give very similar stress–strain curves. Larger tube diameters (or weaker constraints) give the same influence on stress–strain curves as larger relaxations of the microscopic deformations.

To help to clarify these problems we will therefore consider the form factor of network chains for SANS by using the tube concept in the same form as has been recently done for mechanical properties. By this way, new and additional information about the validity of the tube model will be expected.

The paper will be organized in the following manner. First, assumptions and results of the tube model and results of the Warner–Edwards approach to the structure-averaged form factor in combination with the tube model used will be discussed. Then, a short review as

[⊗] Abstract published in *Advance ACS Abstracts,* October 15, 1994.

0024-9297/94/2227-7681$04.50/0

to the current state of the subject on form factors of network chains will be given. Finally, some general predictions of this approach and especially the predicted influence of the strength of the tube constraints and of the deviations between macroscopic and microscopic deformations on the form factor will be discussed and compared with new experimental data obtained on chemically cross-linked networks.

2. The Tube Model

Before we consider the results of the tube model used for the treatment of the SANS data, it seems necessary to recollect some basic problems of the statistical mechanics of polymer networks because the structure averaging in the deformed state is crucial for a successful treatment of such systems.[9,10] Rubberelastic networks are disordered systems with a fixed cross-link as well as entanglement structure. Both are determined by the cross-linking (e.g., vulcanization) process and will not be influenced by deformation until chain or cross-link rupture occurs. The calculation of any measurable quantity for a macroscopic sample with a given distribution of cross-link and entanglement topologies p_T in a deformed state with the deformation tensor λ demands therefore the following averaging procedures:

$$\langle\langle A\rangle\rangle = \sum_{\{T\}} p_T \langle A(\lambda)\rangle_T \tag{1}$$

where $\langle\langle ...\rangle\rangle$ denotes the structure and the thermodynamic averaging whereas $\langle ...\rangle_T$ gives the thermodynamic average for a given topology T. Within the framework of the tube model for a rubberelastic network, the topology T will be characterized by a set of space curves $\hat{\vec{R}}(s)$, where s is the contour variable, and cross-link positions $\hat{\vec{R}}_i$ which can be considered as average configurations or positions. The actual configurations of the chains are denoted in the same way as $\vec{R}(s)$ and $\vec{R}_i$. It is important to note that the deformation enters only into the "thermodynamically" averaged quantities as the free energy and the structure factor for a given topology whereas the structure average has to be performed over the initial probability distribution of the topology. In this way, the consideration of a network as quenched systems allows the determination not only of the average deformations but also of fluctuations about the average configurations and therewith of the topological constraints from scattering data of deformed systems.

We will focus our attention on rubberelastic networks made by random cross-linking of long primary chains. It will be assumed that the constraints acting on any segment of chains are equal. This condition is fulfilled if the average number of cross-links per primary chain is large enough that the segments in dangling ends give small contributions only to the properties of interest and the fluctuations of the cross-link number per primary chain are small in comparison to the average values. Small average numbers of cross-links per primary chain are expected to cause in addition to larger dangling end contributions to the observed quantities also the above-mentioned (and discussed in more detail below) pronounced relaxations of chain configurations toward the undeformed state.

The average number of cross-links per network chain is an important parameter for a rubberelastic network, but as decisive for the applicability of the tube model the number of statistical segments of a network chain, $N_{c,st}$ has to be considered. $N_{c,st}$ should be so large that the number of geometrically neighbored chains, i.e., the Flory number N_f (the number of chains which have segments within the coil volume of a network chain)

$$N_f = (n_{st} l_{st}^3) N_{c,st}^{1/2} \tag{2}$$

is much larger than the number of topologically neighbored chains $2(f-1)$ (n_{st} is the number density of statistical segments of length l_{st} in the network, and f is the functionality of the cross-links). Large values of N_f therefore justify the applicability of the tube model as a mean field approach to the entanglement problem. Then it can be expected that the effect of constraints caused by a large number of chains can be described in a good approximation by a confining potential and the effect of discrete entanglements is of minor importance. Networks obeying the above-discussed condition will be called moderately cross-linked networks. A more extensive discussion is given elsewhere.[1]

Within the tube model the constraints in a rubberelastic network (or in an entangled melt) will be modeled in the following way:

The probability of a configuration $\hat{\vec{R}}(s)$ is given by the random walk distribution

$$p(\hat{\vec{R}}(s)) \sim \exp\{-3/2 l_{st} \int_0^L ds\, (\partial \hat{\vec{R}}(s)/\partial s)^2\} \tag{3}$$

We assume that this distribution has not changed by the cross-linking process.

The constraints caused by neighboring chains are modeled by a harmonic potential. In the deformed state we will assume that this potential is diagonal in the main axis system of the deformation tensor and as conditional probability of the chain configuration results[11]

$$p(\vec{R}(s)|\hat{\vec{R}}(s)) \sim \exp\{-3/2 l_{st} \int_0^L ds\, (\partial \vec{R}(s)/\partial s)^2 - \sum_\mu w_\mu^2 \int_0^L ds\, (R_\mu(s) - \lambda_\mu \hat{R}_\mu(s))^2\} \tag{4}$$

where $\mu = 1,2,3$ are the main axis directions of the deformation tensor.

The potential parameters w_μ were calculated approximately by determining the change of the entropy of the surrounding constraining chains caused by a displacement of a segment of the chain under consideration.[12-14] Using the mean square displacements

$$d_\mu^2 = \langle\langle (R_\mu(s) - \lambda_\mu \hat{R}_\mu(s))^2\rangle\rangle \tag{5}$$

instead of the potential parameters $w_\mu = l_{st}^{1/2}/d_\mu^2$ as a measure of the strength of the constraints, we obtained

$$d_\mu = d_0 \lambda_\mu^{\nu} \tag{6}$$

with $\nu = 1/2$ and

$$d_0/l_{st} = \alpha\, (n_{st} l_{st}^3)^{-1/2} \tag{7}$$

The exponent $\nu = 1/2$ is a result of the above-mentioned mean field approach where the deformations of the constraining chains were described in the main axis system of the deformation tensor in the same way as in eqs 4 and 5. The dependence $d_0 \sim n_{st}^{-1/2}$ obtained is in accordance with the Graessley–Edwards approach,

taking into account only the chainlike nature, given by the so-called contour length density.[15] For the prefactor in the melt case the theoretical value $\alpha_{melt} \simeq 8.5$ was obtained,[13] which yields a very satisfactory agreement with plateau modulus data.[15] For moderately cross-linked networks several approximations resulted in the theoretical value $\alpha_{net} \simeq 5.8$,[14] whereas from experimental data somewhat lower values $\alpha_{net} \simeq 4$ were deduced.[6,7] In a comparative study of models of entanglement constraints which has been published recently,[16] the power close to $-1/2$ in eq 7 was confirmed.

To allow for the strong swelling dependence of the constraint contribution of the network modulus and to explain the small constraint contributions of most of the end-to-end linked networks the concept of reduced microscopic deformations[1] $\lambda_\mu \rightarrow \lambda_{\mu,i}$ was introduced with

$$\lambda_{\mu,i} = \lambda_\mu^{\beta}; \quad 0 \le \beta \le 1 \tag{8}$$

The parameter β can be considered as an empirical parameter which describes the partial relaxation of the chains toward the undeformed state and therewith a relaxation of the deformed tubes toward the undeformed tubes. The definition of the microscopic deformation in this way is arbitrary and assumes the proper limits.

In summarizing this short presentation of the tube model, it should be stated that stress–strain properties depend in such a way on the parameters α and β that an unambiguous determination of both parameters is hardly possible.

3. Form Factor

The theory of the form factor of network chains is well described in several comprehensive reviews.[17–19] Although mainly the case of a labeled network chain is considered in ref 17, i.e., networks made by end-to-end linking of chains, and the influence of heterogeneities are of main interest in ref 18, the general conclusions are of interest also for the systems considered here. In the former[17] the result was confirmed that both "classical" phantom models, the Kuhn–Flory theory with affine junction displacements and the James–Guth approach with free fluctuating junctions, give in a Kratky representation of scattering intensities larger and narrower humps for the scattering properties perpendicular to the stretching direction as reported by available experiments. As a consequence of this behavior, the Flory–Erman model as an interpolation between these limiting cases is disqualified as a possible explanation. Vilgis et al.[20] derived a dynamic as well as a static form factor for a chain permanently linked into a network. The cross-link motion is here treated in terms of a localizing harmonic potential, and good agreement is found with the mean square displacements of cross-links as measured in a spin–echo experiment.[21] Nevertheless, they further showed that an explicit incorporation of entanglements into their approach is equivalent to the Flory–Erman constrained-junction model, which failed in the former analysis.

Recently the James–Guth model was reinvestigated[19] avoiding some approximations made in earlier investigations. The new results show larger humps than originally calculated by Ullman's approximation.[22] A quantitative comparison with experimental data was not made but the authors concluded as in ref 17 that the experimental data show the maxima for perpendicular scattering to be lower and broader,[8,23–28] indicative for lower cross-link densities than estimated.

Using the Warner–Edwards[29] approach as a starting point,[8] it was shown that the deformation of the chains must be less than the macroscopic deformation of the sample. By this assumption a much better agreement between theoretical predictions and scattering data for deswollen networks was achieved but the form of the hump in Kratky plots remained still somewhat different.

Recently also an analytical solution was presented[30] for a model where the entanglements are treated as stress points which undergo an affine deformation. The obtained form factors are similar to the results in ref 19 as has to be expected due to the similarities to the investigated models. Again the predicted maxima for perpendicular scattering are narrower as the experimental data.

Special attention has been devoted[18,31] to the influence of network heterogeneities on scattering properties. We will not consider this problem in detail assuming that in the case of networks made by cross-linking of long primary chains the main type of heterogeneity is the random distribution of cross-links along the chains which is taken into account by the mean field approach used. Large-scale heterogeneities which gave rise to butterfly patterns are not treated here and involve a different structure averaging. In section 2 the large values of the Flory number were discussed as the basis of applicability of the tube model as a mean field approximation to the entanglement problem. We expect from this discussion that for networks made from long primary chains this approximation is adequate in the range of small and moderate strains and the contributions of fluctuations are negligible.

Summarizing this short enumeration of theoretical results, it can be concluded that especially the shape of the maxima of the scattering in the perpendicular direction is not in agreement with experimental data, nor could the scattering be explained in terms of the same number of cross-links in both principal directions of the strain axes.

We will focus attention on the Warner–Edwards[29] approach as the theoretical basis for the calculation of the structure factor of a labeled path in a network, because, by this way, the scattering properties can be calculated using the same assumptions and model parameters as for the stress–strain properties.

The property of interest which has to be structure averaged is the form factor of a labeled path of N_l segments

$$S(\vec{k}) = \frac{1}{N_l^2}\langle \sum_{ij} \exp[i\vec{k}(\vec{R}_i - \vec{R}_j)] \rangle = \langle \Phi_k \rangle \tag{9}$$

Φ_k is therewith the property which has to be averaged according to eq 1. The theory of Warner and Edwards[29] gives for the structure-averaged form factor $S(\vec{k},\lambda)$ in the deformed state

$$S(\vec{k},\lambda) = \frac{1}{N_l^2}\sum_{ij} \exp\left[-(k_\mu \lambda_\mu l_{st})^2 |j-i|/6 - \frac{k_\mu^2 (1-\lambda_\mu^2) l_{st}^{1/2}}{2(6^{1/2})\tilde{w}_\mu}\left(1 - \exp\left(-\frac{2 l_{st}^{3/2}}{6^{1/2}}\tilde{w}_\mu |j-i|\right)\right)\right] \tag{10}$$

Equation 10 is identical with the results in ref 29 but the potential parameter $w_{\mu,c}$ of the phantom problem considered there is replaced by the resulting potential

$\tilde{w}_\mu$ caused by the cross-links and the entanglements.[32] Evaluation of the double sum in eq 10 as an integral gives after introduction of dimensionless chain length coordinates and replacing the potential parameters $\tilde{w}_\mu$ by the corresponding fluctuation parameters $\tilde{d}_\mu$

$$S(\vec{k},\lambda) = 2\int_0^1 dx \int_0^x dx' \prod_\mu \exp\left[-(Q_\mu\lambda_\mu)^2(x-x') - Q_\mu^2(1-\lambda_\mu^2)\frac{\tilde{d}_\mu^2}{2(6^{1/2})R_g^2}\left(1-\exp\left(-\frac{(x-x')}{\tilde{d}_\mu^2/(2(6^{1/2})R_g^2)}\right)\right)\right] \quad (11)$$

where R_g is the radius of gyration of the labeled path and $Q_\mu = k_\mu R_g$ is a component of the reduced scattering wave vector in the main axis system of the deformation tensor. For a description of the results of relaxation processes the components of the deformation tensor λ_μ may be replaced according to eq 8 by the corresponding microscopic deformations.

In the small-$\vec{k}$ limit $Q_\mu \ll 1$ the exponential function in eq 11 can be expanded into a Taylor series. Up to terms in Q_μ^2, $S(\vec{k},\lambda)$ reads

$$S(\vec{k},\lambda) = \prod_\mu \left\{1 - Q_\mu^2\left\{\frac{\lambda_\mu^2}{3} + (1-\lambda_\mu^2)\frac{\tilde{d}_\mu^2}{2(6^{1/2})R_g^2}\left[1 - 2\frac{\tilde{d}_\mu^2}{2(6^{1/2})R_g^2}\left(1 - \frac{\tilde{d}_\mu^2}{2(6^{1/2})R_g^2}\right)\left(1-\exp\left(-\frac{2(6^{1/2})R_g^2}{\tilde{d}_\mu^2}\right)\right)\right]\right\} + ...\right\} = \prod_\mu \left\{1 - \frac{1}{3}Q_\mu^2\left(\frac{R_{g,\mu}}{R_g}\right)^2 + ...\right\} \quad (12)$$

The success of a determination of microscopic quantities as $\tilde{d}_\mu$ or of the parameter β in eq 8 as a measure of relaxation and constraint release processes depends strongly on the sensitivity of the dependence of the predicted measurable properties on these parameters. To get an impression of the dependence of $S(\vec{k},\lambda)$ on the parameters $\tilde{d}_0$ and β, in Figure 1 $S(\vec{k},\lambda)$ is plotted for $\lambda = 1/\sqrt{3}$, 1, and 3 and for values of these parameters which enclose their expected range. It can be seen that the parameters $\tilde{d}_0$ and β have similar effects on $S(\vec{k},\lambda)$ but the shape of the curves along the principal axes of deformation is different enough to allow an unambiguous determination. It is visible that narrower tubes cause broader humps for the scattering properties perpendicular to the stretching direction.

As a first application of the presented theory the parameters are determined which describe the scattering data of Bastide et al.[8] There for polystyrene of very high molecular weight ($M \approx 2.6 \times 10^6$) an isotropic bulk sample, the same sample stretched by the deformation ratio $\lambda = 4.6$, tempered (60 and 600 s) and quenched below T_g, and a network cross-linked in semidilute solution and deswollen by a factor of 10 are investigated. Figure 2 shows the experimental results and the fit curves according to eq 11. The parameters $\tilde{d}_0$, β, and R_g were fitted for each data set independently and are listed in Table 1. Only data in the perpendicular direction are shown for the sake of simplicity.

Table 1 shows that the microscopic deformations in the deswollen network as well as in the stretched melts

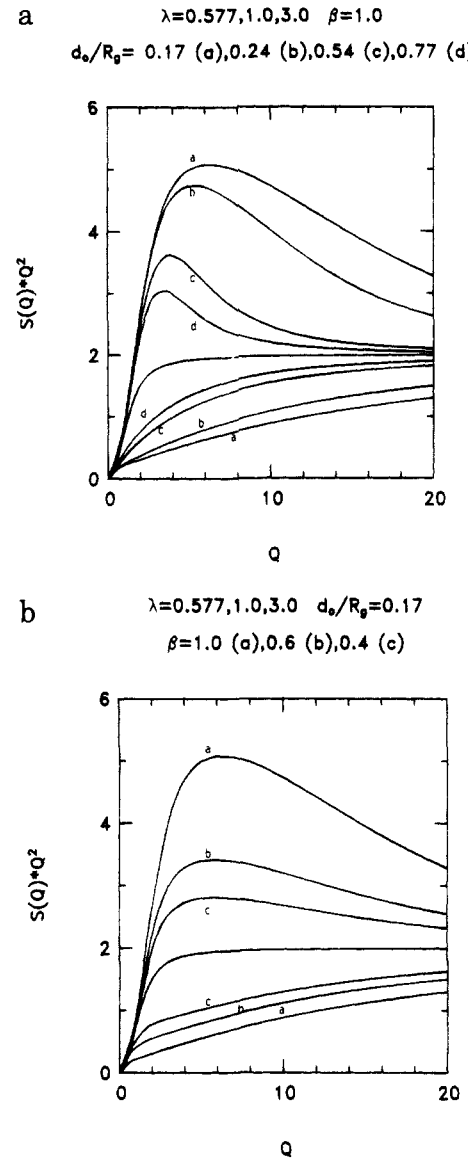

Figure 1. $S(\vec{k},\lambda)$ in Kratky representation for varying fluctuation parameters $\tilde{d}_\mu$ and constraint release parameters β. The isotropic form factor with plateau at 2 is shown as the reference. **Q** is defined as $k \cdot R_g$.

as estimated from β are much smaller than the actual macroscopic deformations. These values agree with the "loss of affineness" discussed in refs 8 and 23. The parameter $\tilde{d}_0/R_g$, on the other hand, compares reasonably well with the expected values, concerning the stretched melts, assuming $\alpha_{melt} = 8.5$ and the appropriate molecular parameters for the statistical segment length. It differs, however, considerably by an order of magnitude in the deswollen network case with $\alpha_{net} = 4$, which predicts $\tilde{d}_0/R_g$ about 0.03, in clear disagreement. An explanation for this striking discrepancy may be found in the overcoiled structure of the deswollen network chains after cross-linking and solvent removal, giving rise to a reduced entanglement density. Given the volume fraction ϕ at cross-linking stage about 0.1, a quick estimate of the number density of segments is then roughly $\phi n_{l_{st}}$. Replacement of this corrected density into eq 7 improves the agreement with experiment considerably and is consistent with an α value at a bulk density of 7.85. Estimated α values in Table 1 are obtained from the fits.

The tendency to smaller values is probably caused by the very large relaxations times of the high molecular

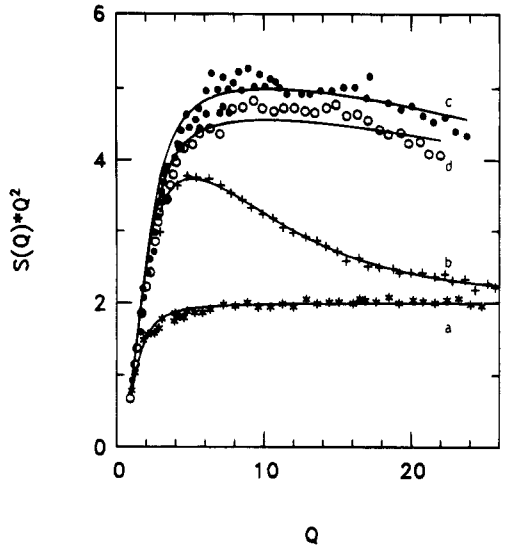

Figure 2. Form factor $S(\vec{k},\lambda)$ of perpendicular direction in Kratky representation for the Bastide experiments of ref 8: (a) isotropic melt; (b) deswollen network; (c) stretched melt, relaxed 60 s; (d) stretched melt, relaxed 600 s. Fit parameters are given in Table 1. **Q** is defined as $k \cdot R_g$.

Table 1. Parameters Describing Bastide's Experiments

sample	R_g/Å	β	$(\bar{d}_0/R_g)_{exp}$	$(\bar{d}_0/R_g)_{th}$	α_{exp}
isotropic melt	333				
deswollen network	386	0.53	0.24	0.030	7.85
stretched melt, 60 s	320	0.63	0.06	0.068	7.50
stretched melt, 600 s	296	0.57	0.06	0.068	7.50

Table 2. Sample Characterization

sample	M_w	M_n	M_w/M_n	method
PB (98% *d*)	75900	70800	1.07	GPC
PB (98% *d*)	70300 ± 7000			SANS[41]
PB (100% *h*)	82300	76950	1.06	GPC

melt samples. The estimated relaxation times in ref 8 are so large that even the characteristic times of the wriggling motion in the melt are of the order of the holding times above T_g of 60 and 600 s. Therefore, the experiments show in Kratky representation mainly a rescaled Debye curve with only a small decrease at higher $\vec{k}$ values because the fluctuation range $\sim d_0$ is not completely accessible within the given times. However, the value extracted experimentally as 91 Å from the network compares very well with the value of 83 Å determined by Graessley.[33] The radius of gyration in the isotropic random walk state of the labeled path was used as an independent fit parameter for each of the curves. The decreasing values with increasing annealing time of the stretched samples can be explained by degradation processes, whereas the larger value of R_g of the network prepared in the swollen state must be considered to be a consequence of the manner of network formation in solution. Chain dimensions of the isotropic melt and stretched melts were found to be identical.

4. Experiments

4.1. Sample Preparation. Butadiene was polymerized anionically in cyclohexane with *s*-BuLi as initiator at 30 °C using standard high-vacuum techniques. Appropriate amounts of protonated and fully deuterated (98% *d*) polybutadiene (Table 2) in benzene ($v_2 = 0.2$) were mixed with a stoichiometric amount of the cross-linking agent BPMTD−(Ad−Ad)$_2$ after which the solvent was pumped off (Ad = Adamantane). Thermal treatment of the blends at 50, 70, and 120 °C caused BPMTD to be set free and (Ad)$_2$ to be sublimed off. The BPMTD then reacted quickly with the double bonds of the polybutadienes to produce an active tetrafunctional cross-link. The conversion is about 90% from mechanical analysis and swelling of the resulting networks.[34] Network parameters for three samples, P14, P15, and P16, for varying amounts of cross-linker are given in Table 3.

Table 3. Network Characterization

sample	ϕ_D	% BPMTD	M_c(chem)	cross-links/chain
P14	0.114	0.117	25600	2.7
P16	0.115	0.150	20000	3.5
P15	0.116	0.225	13300	5.3

4.2. SANS. Small-angle neutron scattering experiments were performed mainly at KWS1 and KWS2 at the FRJ-2 reactor in KFA, Jülich, at wavelengths λ_N = 5.52 and 6.72 Å with $\Delta\lambda_N/\lambda_N = 0.18$. Data were obtained from crossed BF_3 countertubes along the parallel and perpendicular strain directions at different sample-to-detector positions, covering a scattering vector range $0.008 \le k \le 0.14$ Å^{-1}. The networks were stretched symmetrically in a calibrated straining apparatus. Affinity in the macroscopic deformation was assumed throughout, and thicknesses were calculated as for an incompressible sample.

4.3. Data Treatment. Two different evaluations were undertaken. In the first evaluation, emphasis was on the small-$\vec{k}$ data and independent information was needed. Corrections for slightly mismatched molecular weights in the form factors were neglected. Since the cross-linking reaction proceeded in the bulk phase, also the nonideality of the blend (11% *d*/89% *h*) had to be taken into account in that we adopted a calculated Flory−Huggins term by Bates[35] as $\chi = (1.11 \pm 0.25) \times 10^{-3}$ for the same microstructure.

The observed differential cross section, $d\Sigma/d\Omega(\vec{k})$ for an ideal blend, is related to the form factor $S(\vec{k})$ by

$$\frac{d\Sigma}{d\Omega}(\vec{k}) = \left(\frac{\Delta\varrho^2}{N_A}\right) S(\vec{k}) \tag{13}$$

$\Delta\varrho^2$ being the contrast factor, given by $N_A[n(b_D - b_H)/\Omega_0]^2$. b_H and b_D are the nuclear coherent scattering lengths for hydrogen and deuterium, and n is the number of exchanged hydrogens per monomer of molar volume Ω_0. In the Zimm representation, the RPA method including a χ term then reads

$$\left(\frac{d\Sigma}{d\Omega}(\vec{k})\right)^{-1} = \left(\frac{N_A}{\Delta\varrho^2}\right)\left[S(\vec{k})^{-1} - \frac{2\chi}{\Omega_0}\right] \tag{14}$$

Further, a procedure by Ullman[36] to correct the Zimm approximation for larger $k \cdot R_g$ was used, for which we refer to the literature. Details of the data evaluation have been presented elsewhere.[37] The average molecular weight, derived from the forward scattering at $\vec{k}$ = 0, was (68950 ± 2000), in excellent agreement with our former data[41] and GPC values, proving that the assumptions made for χ were reasonable. $\langle R_g \rangle_w$ in the networks is (116 ± 5) Å. Ratios of radii of gyration of the strained chains were compared to theory using the small-$\vec{k}$ approximation of eq 13.

In the second evaluation, the data were also fitted over the complete scattering vector range by means of the presented form factors. For the isotropic case, using the RPA correction for chains with equal molecular weight the Debye curve for Gaussian coils was fitted to

Table 4. Parameters Describing the Experiments[a]

sample	$R_{g,w}$/Å Zimm	Debye	Kratky	β	$(\bar{d}_0/R_g)_{exp,s}$	$(\bar{d}_0/R_g)_{th,\alpha=8.5}$
P14	111(3)	112(5)	116(3)	0.35	0.36	0.34
P16	113(3)	107(4)	113(4)	0.56	0.35	0.34
P15	123(3)	118(4)	118(3)	0.84	0.35	0.34

[a] Standard deviations are given in parentheses.

Table 5. Radii of Gyration as a Function of Strain

sample	λ	$R_g^{\parallel}$ Zimm	$R_g^{\perp}$ Zimm	$R_g^{\parallel}/R_g^0$ Zimm	$S(k)$	$R_g^{\perp}/R_g^0$ Zimm	$S(k)$
P14	1.00	108	114	1.00	1.00	1.00	1.00
	1.30	118	111	1.09	1.07	0.98	0.95
	1.68	130	107	1.20	1.16	0.94	0.91
	1.90	133	105	1.23	1.20	0.92	0.89
P15	1.00	123	123	1.00	1.00	1.00	1.00
	1.09	131	121	1.07	1.05	0.99	0.97
	1.41	151	119	1.23	1.26	0.96	0.86
P16	1.00	116	110	1.00	1.00	1.00	1.00
	1.35	130	109	1.12	1.14	0.99	0.91
	1.58	137	106	1.18	1.22	0.97	0.88

give $R_{g,z}$, the forward scattering $d\Sigma/d\Omega(0)$, and a best-fit effective Flory–Huggins parameter. For the networks P14, P15, and P16, we obtained $\chi = 4.50 \times 10^{-3}$, 3.03×10^{-3}, and 4.65×10^{-3}, respectively. The average $\langle R_g \rangle_z$ and M_w were (121 ± 3) Å and (75000 ± 4000) in this case. No corrections for the poorly extended small-$\vec{k}$ range were necessary here. Absolute values for χ are comparable and only influence the Guinier region.

The fit of the experimental data by eq 11 was performed by evaluation of the double integral with the help of the IMSL routine TWODQ and minimization of the discrepancy between the fit curve and the experimental points in the Kratky representation using the IMSL routine UMPOL. R_g, $\bar{d}_0/R_g$ and β are the independent fit parameters.

5. Results and Discussion

The experimental radii of gyration of the isotropic samples in Tables 4 and 5 can now be compared to literature data in terms of molecular quantities such as C_∞ and the Kuhn segment length l_{st} from which again the necessary packing parameters or segment number densities n_s can be estimated.

From the measurements on the unstrained network the parameters of the coil structure of the chains were deduced for comparison with literature values. Taking into account the microstructure, disregarding the thermal treatment in order to initiate the cross-linking process, the number of bonds n_b per monomer reduces to 3.72 instead of 4 due to the presence of 7% vinyl side groups. The mean number of monomers per chain N_{mono} from the absolute calibration is (1277 ± 117), which allows us to calculate C_∞ via the relation

$$C_\infty = 6R_{g,w}^2/(N_{mono} n_b l_0^2) \qquad (15)$$

where l_0 stands for the average bond length in the monomer.

Special care must be taken, however, when data from different evaluations are combined since effects of polydispersity, background, Flory–Huggins terms, and even weighting schemes may affect the data in several ways. Polydisperse coils always give z averages of radii of gyration for which one can correct easily if an assumption about the distribution is made. Flory–Huggins interactions only appear in the smallest $\vec{k}$ range and mainly affect the forward scattering whereas

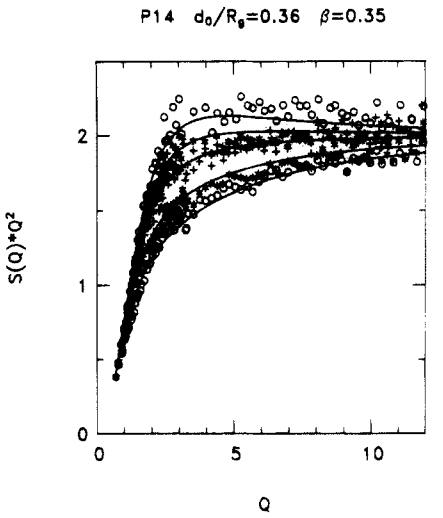

Figure 3. $S(\vec{k},\lambda)$ for sample P14 in Kratky representation and corresponding best-fit curves with parameters in Table 4. From top to bottom: $\lambda_{\parallel} = 1.68$, $\lambda_{\parallel} = 1.30$, $\lambda = 1.0$, $\lambda_{\perp} = 0.88$, $\lambda_{\perp} = 0.77$. **Q** is defined as $k \cdot R_g$.

background subtraction changes the expected $\vec{k}^{-2}$ dependence in Kratky representations.

Data at the lowest $\vec{k}$ were, as stated, corrected by the Ullman procedure, which yields immediately weight averages, $R_{g,w}$. A pronounced dependence on cross-link density is observed. Extrapolation to zero cross-link concentration yields $R_{g,w}$ = (97 ± 6) Å, in close agreement with a previous estimate from a melt sample, which was (98 ± 1) Å. From this fact, we conclude that the coil expansion with increasing cross-linker concentration is caused by the rodlike shape of the cross-linker (L = 15 Å, ϕ = 10 Å) and its stiffness. As in nematic polymers, such a rodlike component may induce some partial orientational interactions and therewith a coil expansion.

Data from the higher scattering vector range yield $R_{g,z}$ values which are converted to the weight averages using the relation $R_{g,z}^2 \sim M_z$ and $M_z = M_w(1 + u)$. The scatter of the data is large but as seen from Table 4, about the same coil dimensions are derived within error limits, although the systematic rise of R_g with increasing cross-link density is perturbed by the scatter. Additionally, a fit of the data weighted with $\vec{k}^{-2}$ according to the Kratky plot is made. The agreement with the data obtained from the Zimm region is satisfactory. This proves that especially the background corrections are done correctly.

C_∞ as obtained from the extrapolation is (5.4 ± 0.6) where the estimated error is primarily determined by the uncertainty of the absolute calibration. The established value for atactic polybutadienes with the same vinyl content is 5.5 from measurements in Θ solutions.

From these values the statistical segment length for the equivalent model chain $l_{st} = C_\infty l_0$ = (8.0 ± 0.9) Å, and M_s, its mass, is analogously given by $C_\infty m_0$ = (75 ± 10). m_0 is the mass assigned to a CH_2 unit of the backbone chain. The density of statistical segments as defined earlier by $n_s = \varrho N_A/M_s$ is (7.23 ± 0.92) × 10^{21}/cm^3. The number of segments in a cube of length l_{st} (reduced segment density) is then $(n_s l_{st}^3)$ = (3.7 ± 1.4), and an independent test of the prefactor α in eq 7 can now be performed when $\bar{d}_0$ is known.

In the strained networks, eq 11 shows that the scattering should be entirely explained in terms of only two quantities, β and $\bar{d}_0/R_g$. Figures 3–5 present the results of the fit of the experimental data by means of

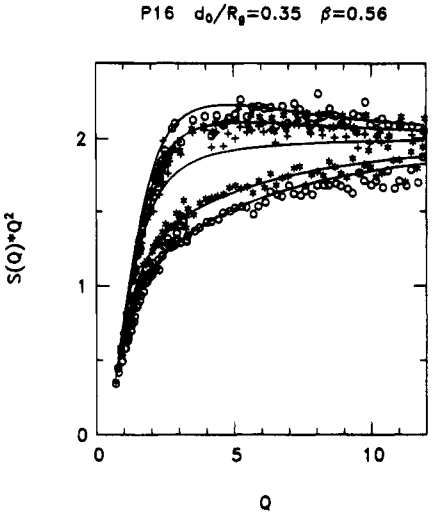

Figure 4. $S(\vec{k},\lambda)$ for sample P16 in Kratky representation and corresponding best-fit curves with parameters in Table 4. From top to bottom: $\lambda_{||} = 1.58$, $\lambda_{||} = 1.35$, $\lambda = 1.0$, $\lambda_\perp = 0.86$, $\lambda_\perp = 0.79$. **Q** is defined as $k \cdot R_g$.

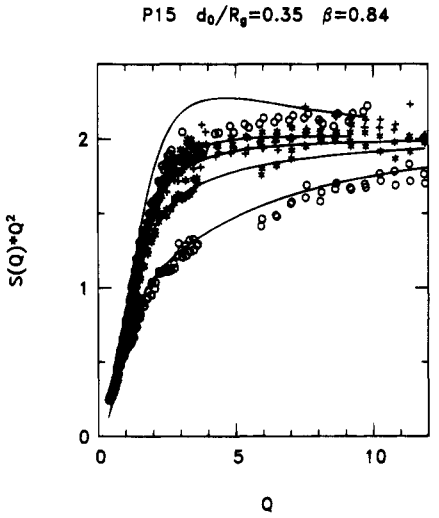

Figure 5. $S(\vec{k},\lambda)$ for sample P15 in Kratky representation and corresponding best-fit curves with parameters in Table 4. From top to bottom: $\lambda_{||} = 1.41$, $\lambda_{||} = 1.09$, $\lambda = 1.0$, $\lambda_\perp = 0.96$, $\lambda_\perp = 0.84$. **Q** is defined as $k \cdot R_g$.

the form factor. The data at all strains are consistent with one set of parameters, R_g, $\tilde{d}_0$, and the constraint release exponent β. The discrepancy for the largest strain in sample P15 is probably due to an erroneous incoherent background which itself was optimized at the unstrained sample and to which the Kratky representation is severely sensitive. The fits yielded values for β varying between 0.35 and 0.84 and an average tube parameter $\tilde{d}_0/R_g = (0.353 \pm 0.006)$. The fluctuation range therefore is $\tilde{d}_0 \sim (41 \pm 1)$ Å based on the measured network chain dimensions. The dynamic plateau modulus in the Doi–Edwards approach yielded 35 Å, which implies that the freedom of motion on the segmental level is not noticeably changed by the network topology. Taking the extrapolated value for R_g as the reference, $\tilde{d}_0$ is derived as (34 ± 1) Å.

The prefactor α_{net}, introduced in eq 7, is calculated from $\tilde{d}_0$ and the reduced segment density considered above and gives (8.2 ± 0.8), very close to the value predicted for melts.

Because often only small-angle scattering data are available, also the sensitivity of the form factor in the Zimm region to the tube parameters was tested. It is

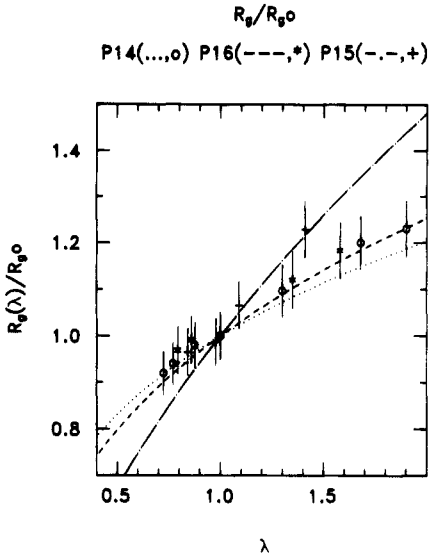

Figure 6. Chain deformations $R_{g,\mu}/R_g$ for network samples and calculated best-fit curves with parameters obtained from Table 4.

clear that the Zimm approximation is inferior since terms in $\tilde{d}_0/R_g$ only contribute approximately 5%. Therefore, the tube parameter is only roughly estimated as (0.31 ± 0.1). The fit curves in Figure 6 are calculated using the parameters obtained from fitting the whole $\vec{k}$ range. The agreement is satisfactory and would be increased if two-dimensional fits would have been available.

At this point a comparison with the tube confinement parameters obtained from mechanical analysis is to be made. Only limited information on the samples under investigation was available which yielded tube diameters between 25 and 35 Å. Another source of data, obtained on *cis*-polybutadiene radiation-cross-linked networks with much longer primary chains ($M_w \approx 3.0 \times 10^5$)[38] yielded $\tilde{d}_0 \sim 32$–34 Å in the range of network chains M_c used here, assuming $\beta = 1.0$, however. Smaller tubes are obtained in the case of higher cross-linking densities favoring $\alpha_{net} = 4$ in ref 6. The stronger dependence of the tube parameter in stress–strain data is not yet clear. Possibly different mechanisms of the contribution of segmental fluctuations to the observable quantities are responsible. Also, dynamic contributions, due to the finite strain velocity at stress monitoring may simulate stronger hindrances and therefore a narrowing of tubes. The effect of primary chain length, which may influence constraint release processes and causes different contributions of undeformed dangling chain ends, is to be dealt with in more detail in forthcoming studies.

Summarizing the results, it can be stated that the tube approach with deformation-dependent constraints gives, for moderately dense cross-linked rubberelastic networks made from long primary chains, a very satisfactory description of the small-angle neutron scattering properties in the range of moderate deformations. The fit of the experimental results with the help of the given theory yields tube dimensions which are in reasonable agreement with data derived from stress–strain behavior using the same theoretical background. However, the tube dimensions from SANS are closer to the values obtained by estimations of tube dimensions using viscoelastic measurements on melts.

As a second result the loss of affineness as postulated already[8] and its dependence on the network parameters were confirmed. Relatively weakly cross-linked net-

works gave constraint release parameters β considerably less than 1. Consequently, it has to be taken into account that relaxations and fluctuations are very important in the investigated samples.

The form factor gained special importance in the observation that a quantity as the displacement of a chain segment of the constrained chain under consideration $\tilde{d}_0$ observed up to now only by dynamical experiments seems to be readily accessible from the measurement of the static form factor. Although a tube approach was proposed already by Boue et al.[42] for the test of reptation of deformed chains in melts, the model at hand is the first to evaluate directly the segmental fluctuations in an elegant way and therefore complements a neutron spin–echo study,[39,40] which is used commonly to prove the additional "length" of interest in entangled systems. The reason for this possibility is the quenched structure average which is performed by a scattering experiment on a deformed network.

For more severe tests of the tube model, SANS measurements at larger extensions of networks with a larger number of cross-links per primary chain and variations of the parameter $\tilde{d}_0/R_g$ by variation of the length of the labeled path are necessary. New experiments on polyisoprene as well as polybutadiene networks are under way.

Acknowledgment. We thank the late G. Pohl for his help with the SANS instrument and M. Hintzen and F. Forster for the mechanical characterization of the samples. We are grateful to Prof. W. Gronski (University of Freiburg) for letting us use the data in a revised form and to Dr. G. Meier (MPI Mainz) for performing some test experiments at the twin KWS2 instrument.

References and Notes

(1) Heinrich, G.; Straube, E.; Helmis, G. *Adv. Polym. Sci.* **1988**, *85*, 33.
(2) Edwards, S. F.; Vilgis, T. A. *Rep. Prog. Phys.* **1988**, *51*, 243.
(3) Vilgis, T. A. *Kautsch. Gummi, Kunstst.* **1989**, *42*, 475.
(4) Abramchuk, S. S.; Nyrkova, I. A.; Khokhlov, A. R. *Vysokomol. Soedin.* **1989**, *31*, 1759.
(5) Straube, E.; Heinrich, G. *Kautsch. Gummi, Kunstst.* **1991**, *44*, 734.
(6) Matzen, D.; Straube, E. *Colloid Polym. Sci.* **1992**, *270*, 1.
(7) Gronski, W.; Hoffmann, U.; Simon, G.; Wutzler, A.; Straube, E. *Rubber Chem. Technol.* **1992**, *65*, 63.
(8) Bastide, J.; Herz, J.; Boué, F. *J. Phys. (Paris)* **1985**, *46*, 1967.
(9) Ziman, J. M. *Models of Disorder*; Cambridge University Press: Cambridge, 1979.
(10) Freed, K. F. *Adv. Chem. Phys.* **1972**, *22*, 1.
(11) Edwards, S. F. Statistical Mechanics of Rubber. *Polymer Networks: Structural and Mechanical Properties*; Plenum Press: New York, 1971.
(12) Heinrich, G.; Straube, E. *Acta Polym.* **1983**, *34*, 589.
(13) Heinrich, G.; Straube, E. *Acta Polym.* **1984**, *35*, 115.
(14) Heinrich, G.; Straube, E. *Polym. Bull.* **1987**, *17*, 247.
(15) Graessley, W.; Edwards, S. F. *Polymer* **1981**, *22*, 1329.
(16) Richter, D.; Farago, B.; Butera, R.; Fetters, L. J.; Huang, J. S.; Ewen, B. *Macromolecules* **1993**, *26*, 795.
(17) Vilgis, T. A.; Boué, F. *Polymer* **1985**, *27*, 1154.
(18) Vilgis, T. A. In *Elastomeric Polymer Networks*; Prentice-Hall: Englewood Cliffs, NJ, 1992.
(19) Kloczkowski, A.; Mark, E.; Erman, B. *Comput. Polym. Sci.* **1992**, *2*, 8.
(20) Vilgis, T.; Boué, F. *J. Polym. Sci., Polym. Phys. Ed.* **1987**, *26*, 2291.
(21) Richter, D.; Ewen, B.; Oeser, R. In *Polymer Motions in Dense Systems*; Richter, D., Springer, T., Eds.; Springer-Verlag: Berlin, 1988.
(22) Ullman, R. *Macromolecules* **1982**, *15*, 1395.
(23) Bastide, J. In *Physics of Finely Divided Matter*; Springer Proceedings in Physics 5; Springer: Berlin, 1985.
(24) Higgs, P. G.; Ball, C. *J. Phys. (Paris)* **1988**, *49*, 1785.
(25) Boué, F.; Bastide, J.; Buzier, M.; Colette, C.; Lapp, A.; Herz, J. *Prog. Colloid Polym. Sci.* **1987**, *75*, 152.
(26) Picot, C. *Colloid Polym. Sci.* **1987**, *75*, 83.
(27) Boué, F.; Farnoux, B.; Bastide, J.; Lapp, A.; Herz, J.; Picot, C. *Europhys. Lett.* **1986**, *1*, 637.
(28) Boué, F. *Adv. Polym. Sci.* **1987**, *82*, 1.
(29) Warner, M.; Edwards, S. F. *J. Phys. A* **1987**, *11*, 1649.
(30) des Cloizeaux, J. *J. Phys. (Paris)* **1993**, *4*, 539.
(31) Vilgis, T. A. *Macromolecules Polym.* **1992**, *25*, 399.
(32) Heinrich, G.; Straube, E. *Polym. Bull.* **1987**, *17*, 255.
(33) Graessley, W. *J. Polym. Sci., Polym. Phys. Ed.* **1980**, *18*, 27.
(34) Forster, F. Ph.D. Thesis, Freiburg, 1990.
(35) Bates, F. S.; Wignall, G. D.; Koehler, W. C. *Phys. Rev. Lett.* **1985**, *55*, 2425.
(36) Ullman, R. J. *Polym. Sci., Polym. Phys. Ed.* **1985**, *23*, 1477.
(37) Forster, F.; Pyckhout-Hintzen, W.; Springer, T.; Gronski, W., in preparation.
(38) Pyckhout-Hintzen, W.; Mueller, B.; Springer, T. *Makromol. Chem., Macromol. Symp.* **1993**, *76*, 121.
(39) Butera, R.; Fetters, L. J.; Huang, J. S.; Richter, D.; Pyckhout-Hintzen, W.; Zirkel, A.; Farago, B.; Ewen, B. *Phys. Rev. Lett.* **1991**, *66*, 2088.
(40) Higgins, J. S.; Roots, J. E. *J. Chem. Soc., Faraday Trans.* **1981**, *81*, 757.
(41) Pyckhout-Hintzen, W.; Springer, T.; Forster, F.; Gronski, W.; Frischkorn, C. *Macromolecules* **1991**, *24*, 269.
(42) Boué, F.; Osaki, K.; Ball, R. C. *J. Polym. Sci., Polym. Phys. Ed.* **1985**, *23*, 833.